Evaluation of thermal conductivity and its structural dependence of a single nanodiamond using molecular dynamics simulation

doi: 10.1016/j.diamond.2019.107669

Evaluation of thermal conductivity and its structural dependence of a single nanodiamond using molecular dynamics simulation

Hiroki Matsubara[1)], Gota Kikugawa[1)], Takeshi Bessho[2)], and Taku Ohara[1)]

[1] *Institute of Fluid Science, Tohoku University, 2-1-1 Katahira, Aoba-ku, Sendai, 980-8577 Japan*

[2] I*nstitute of Innovation for Future Society, Nagoya University, Furo-cho, Chikusa-ku, Nagoya, 464-8603 Japan*

[a)] Electronic mail: matsubara@microheat.ifs.tohoku.ac.jp

ABSTRACT

In the present study, we investigated thermal conductivity and its structural dependence of a spherical nanodiamond with 2.5 nm in diameter using molecular dynamics simulation. We briefly discussed the difficulty of computing the thermal conductivity of a free nanoparticle using conventional methods and here we derived it from the non-equilibrium molecular dynamics simulation of a composite system where a nanodiamond is sandwiched between two solid blocks. The structural dependence was examined by applying this method based on a composite system to the 2.5 nm nanodiamonds having different ratios of 3- and 4-coordinate carbons (termed sp^2-like and sp^3-like carbons, respectively), which were obtained from annealing at different temperatures. The thermal conductivity of the nanodiamond decreased from 28 to 10 W/(m·K) with decreasing ratio of sp^3-like carbons until the number of sp^2-like bonds exceeded that of sp^3-like bonds. When sp^2-like bond became richer than sp^3-like bond, the thermal conductivity was less sensitive to further increase of the ratio of sp^2-like carbons. Based on the consideration of the heat transfer associated with a single C–C bond, we interpreted that this structural dependence reflects the heat transfer characteristics of sp^3- or sp^2-like bond, whichever is more abundant. This interpretation, as well as the methodology, is helpful for understanding thermal conductivity of nanodiamonds and other carbon nanomaterials.

1. INTRODUCTION

Nanoparticles of diamond are a promising candidate for a nano-filler aiming at controlling the thermophysical [1] and mechanical [2] properties of nanofluids and nanocomposites. Among others, the modification of thermal conductivity has been extensively considered in view of thermal management in devices with high density of heat generation [1]. The thermal conductivity of such a composite material is often estimated from those of filler and base matrix with the aid of effective medium theories [3]. This estimation requires the thermal conductivity of a single nanodiamond (ND) and base matrix, as well as the thermal contact conductance at the interface between an ND and base matrix. Thermal contact conductance, which depends on the specific type of base matrix, must be taken into account when one evaluates the effective thermal conductivity of a nanocomposite. However, in the present study, as a first step, we focus on the thermal conductivity that is intrinsic to ND. It is of interest to consider how we can extend the concept of thermal conductivity to a nanoscale material.

NDs are most commonly generated by a detonation and typically have a near spherical shape of 2–5 nm in diameter with the most stable size being considered to be 4–5 nm [4,5]. An ND is in general composed of the inner core of diamond lattice and the outer shell of sp^2 carbons and the fraction of sp^2 carbons increases by annealing at a high temperature. Indeed, experiments have shown [6–9] that at 1200–2000 K, ND is transformed into a carbon onion, composed of concentric shells of sp^2 carbons with a quite small diamond core. The formation process of carbon onion has been extensively investigated using molecular dynamics (MD) simulations [4,10–13]. These structural properties can affect the thermal conductivity. In addition, the diameter of 2–5 nm is several orders of magnitude smaller than the typical phonon mean-free-path in bulk diamond, which is roughly estimated to be of the order of 0.1–1 μm at room temperature [14]. It is known that the heat transfer in such a case is mostly ballistic rather than diffusive. That is, the value of thermal conductivity is significantly dependent on the phonons propagating from one end of an ND to the other without being scattered and thereby thermal conductivity shows a

remarkable system-size dependence [15].

Molecular dynamics simulation is a suitable tool for evaluating the thermal conductivity of an ND along with its structure and size, while it is difficult for experiments to measure the thermal conductivity of a single ND. There are two matured methodologies for the MD calculation of thermal conductivity, i.e., the equilibrium MD (EMD) and the non-equilibrium MD (NEMD) under a stationary thermal gradient, which are also called the Green–Kubo method and the direct method, respectively [16]. Although these methods are well-established for bulk materials, care must be taken when one applies them to the system of a free nanoparticle. The EMD method derives thermal conductivity by time-integrating the heat flux autocorrelation function (HACF) up to the timepoint when the HACF converges to zero. Mahajan et al. [17] applied the EMD method to silica nanoparticles and concluded that the EMD method was unsuitable because the HACF has a large and long-lasting oscillation and does not converge within a simulation of acceptable time length. In our view, the EMD method is in principle inapplicable to a nanoparticle, not just because of computational cost. This is because a heat flow and that reflected at the boundary of nanoparticle cancel with each other. As a result, the integrated HACF becomes zero after a characteristic time and the thermal conductivity cannot be determined. We briefly demonstrate this deficiency of EMD method in Appendix A, because it has not been documented clearly in literature.

The NEMD method also has an issue to be solved, as Termentzidis et al. pointed out [18]. The method requires to locate two separate sub-volumes in a nanoparticle as a hot heat source and a cold heat source. Energy is injected into the hot source at a constant rate and the same amount of energy is removed from the cold one to generate a constant temperature gradient between these sub-volumes, from which thermal conductivity is derived using the Fourier law. For example, Mahajan et al. [17] chose the shell and the core of the nanoparticle as the hot and cold sources, respectively. Since these heat sources forcibly scatter phonons, thermal conductivity is significantly underestimated in the regime of ballistic heat transfer. Thus, the conventional methods cannot be used as they are to evaluate the thermal conductivity of a single ND.

In the present study, we employed the NEMD simulation of a composite system where a spherical ND of 2.5 nm in diameter was sandwiched between two copper crystal blocks to evaluate its thermal conductivity. The problem of artificial phonon scattering in the NEMD method can be removed by placing the heat sources within the crystal blocks. In order to discuss the structural dependence, this method was applied to 2.5 nm diamonds having different ratios of 3-coordinate (sp^2-like) and 4-coordinate (sp^3-like) carbons, which were obtained from annealing at different temperature. Thermal conductivity of bulk diamond was also calculated for comparison. Although the present study aims to investigate the thermal conductivity of an ND and its structural dependence, we put another emphasis on the methodological aspect since the MD evaluation of thermal conductivity is not well-established for nanoscale materials. Experiments have shown that in an actual detonation process, various kinds of surface functional groups, typically composed of C, O, and H atoms, can be introduced on the surface of ND [19,20] and the effect of such surface modification is an interesting topic. However, as the most fundamental case, here we consider NDs composed of carbon atoms only.

2. METHOD

2.1 MD simulation of bulk diamond

All MD simulations in the present study were conducted using LAMMPS [21]. The interaction among carbon atoms was modeled with AIREBO potential [22], which reasonably describes the breaking and formation of a C–C bond within the framework of classical MD simulation. AIREBO potential considers the van der Waals attraction among non-bonded atoms and this feature differentiates AIREBO from other common reactive force fields, such as Tersoff [23] and Brenner [24] potentials. We first computed the thermal conductivity of bulk diamond as a reference to be compared with those of NDs

since the diamond thermal conductivity using AIREBO potential has been rarely reported. We derived it from an equilibrium MD of a cubic system composed of 7 × 7 × 7 diamond unit cells (N = 2744 carbon atoms) with the three-dimensional periodic boundary conditions. The equation of motions for all of *NVE*, *NVT*, and *NpT* runs in the following were solved using the algorithm of Tuckerman et al. [25] with a timestep Δt = 0.5 fs. The system size and temperature were relaxed by a 5 ns constant *NpT* run at 1 atm and 298 K followed by a 2 ns constant *NVT* run at 298 K. The lattice constant was relaxed to 3.564 Å by the *NpT* run. Then, the heat flux vector $\mathbf{J}_Q$ was recorded during a 25 ns *NVE* run, from which thermal conductivity λ was calculated using the Green–Kubo relation. Specifically, the 25 ns run was divided into five 5 ns blocks. For each 5 ns block, we computed the running thermal conductivity $\lambda(t)$ as

$$\lambda(t) = \frac{V}{3k_{\mathrm{B}}T^2}\int_0^t \left\langle \mathbf{J}_Q(0)\cdot\mathbf{J}_Q(\tau)\right\rangle d\tau\,, \tag{1}$$

where T is the absolute temperature, V is the system volume, k_{B} is the Boltzmann constant, $\mathbf{J}_Q$ is heat flux, and $\left\langle \mathbf{J}_Q(0)\cdot\mathbf{J}_Q(\tau)\right\rangle$ is the HACF at time difference τ. The thermal conductivity λ was determined as the time average of $\lambda(t)$ for $150 \le t \le 200$ ps, following Fan et al. [26] who calculated the thermal conductivity of diamond crystal with Tersoff potential. The final value of the thermal conductivity was obtained as the average over the five blocks and its statistical uncertainty was estimated as $\sigma(\lambda)/\sqrt{5}$, where $\sigma(\lambda)$ is the standard deviation of the five values of λ. In order to examine the size effect, we also calculated the thermal conductivity for the 10 × 10 × 10 system containing N = 8000 atoms using the same procedure.

It is necessary to mention the calculation of heat flux. LAMMPS (as of version 5 Jun 2019) uses an approximate equation for computing heat flux, which does not guarantee energy conservation law. Recent studies have shown that this approximation is inappropriate for many body potentials except for two-body ones [26–28]. Therefore, we modified the source code of LAMMPS so that heat flux is calculated based on the formula that was appropriately derived from energy conservation. The expression and validation of the modified formula are described in Appendix B. Our modified source code is available at https://github.com/matsubara0/lammps.

2.2 Generation of graphitized nanodiamonds

The NDs having different internal structures were obtained as follows. A spherical nanoparticle with 2.5 nm in diameter and consisting of 1442 carbon atoms was cut out of diamond crystal with a lattice constant $a = 3.567$ Å. This spherical ND was put alone in an MD system with the free boundary conditions in the x, y, and z directions. For the simulations of NDs, timestep was set to $\Delta t = 0.1$ fs. After a short equilibration for 1 ns at 298 K with velocity scaling, the system temperature was raised by velocity scaling up to an annealing temperature T_{anneal} and a 20 ns *NVT* run [25] was conducted. Here, we considered different values of T_{anneal} from 400 K to 3000 K at 200 K intervals, in addition to the case without annealing, which will be referred to as the case of $T_{\mathrm{anneal}} = 298$ K hereafter for convenience. Different structures were obtained since the graphitization, i.e., the breaking of C–C bonds, proceeds more as T_{anneal} increases. The temperature was then scaled back to 298 K and the system was equilibrated with a 12 ns *NVT* run. During the last 4 ns of this *NVT* run, we recorded the positions and velocities of the atoms. These data were used for the structural analysis of the nanoparticle.

2.3 NEMD simulation for the composite system

The thermal conductivity of a single ND was measured by performing the NEMD simulation of a composite system in which an ND is sandwiched by two solid blocks as shown in Fig. 1. The solid blocks were introduced to avoid direct heating of the ND when a thermal gradient is imposed. The sandwiched configuration ensures that the heat flow from one solid block to the other necessarily passes through the ND, which is helpful in estimating the heat flux inside the ND. Any kind of solid species can be used as the solid block; here, we chose copper fcc crystal. The interaction among Cu atoms were modeled by MEAM potential [29] whereas the Cu–C interaction was described by the Lennard-Jones (LJ) potential

using the distance parameter σ_{CuC} = 2.873 Å, energy parameter ε_{CuC} = 0.636 kcal/mol, and cutoff length 12 Å. These LJ parameters were the Lorentz–Berthelot combination of the LJ parameters for C [30] and Cu [31] atoms in accordance with other MD studies on copper–carbon interfaces [32].

This composite system was constructed as follows. We embedded the ND annealed as described in Section 2.2 into the center of an fcc copper crystal of 12 × 12 × 36 unit cells with lattice constant of 3.613Å, where Cu atoms within σ_{CuC} of any C atom were removed. The initial dimensions of the MD box were $L_x \times L_y \times L_z = 43.356 \times 43.356 \times 130.68$ Å^3 and the three-dimensional periodic boundary conditions were imposed. These values of L_x and L_y ensure that carbon atoms in the ND do not interact through the periodic boundary conditions. In addition, as will be discussed in Sec. 3.1, we carried out the same NEMD simulation for T_{anneal} = 298 K using copper blocks twice in length in the z direction to confirm that the z-dependence is sufficiently small. The center of the ND in the z direction was initially $z_c = L_z/2$. In addition, we deleted Cu atoms in the range $|z-z_c| < d/5$ (=5 Å) to create the gap region. After the system was relaxed by an 1 ns NpT run at 298 K and 1 atm, where L_x, L_y, and L_z were allowed to change independently, we elongated L_z to the left and right each by 10 Å to separate the regions that will be used as the hot and cold sources. After the elongation, the stress in the z direction was shortly relaxed again by a 0.5 ns NVT run at 298 K, where a constant force, $f_{const} = p_z L_x L_y / n_a$, inward in the z direction, was applied on each Cu atom in the left and right outermost layers, where p_z = 1 atm and n_a is the number of atoms in each outermost layer.

Subsequently, we performed a NEMD simulation using EHEX algorithm [33]. As shown in Fig. 1, the 2nd to 7th outermost layers on the left and right Cu blocks were defined as the hot and cold sources, respectively, whereas the outermost layers were completely frozen. Every time step, we injected energy into the hot source at the rate of $\dot{E} = 5.667 \times 10^{-8}$ W and removed at the same rate from the cold source to produce a stationary heat conduction in the z direction. The data for analysis was sampled for 30 ns after a 10 ns relaxation run brought the system to a non-equilibrium steady state.

Here, we assumed that thermal conductivity λ is spatially uniform inside the ND whereas heat

flux $J_{Q,z}(z)$ and temperature gradient $\nabla_z T(z)$ are z-dependent according to the z-dependence of x–y cross section, $S_{xy}(z) = \pi\left[(d/2)^2 - (z - z_c)^2\right]$, for a sphere with diameter d = 2.5 nm centered at $z = z_c$. Since the boundary surface of our ND is spherical, heat flux and temperature can also be x and y-dependent. However, we assume one dimensional property in the z direction for heat flux and temperature by considering that these variables are spatially averaged in the x and y directions. The same applies to the heat flux and temperature profiles in the copper block near the contact area with the ND. For the gap region, i.e., $z_c - d/5 \le z \le z_c + d/5$, there is no heat flow through the ND surface and heat flux can be written as $J_{Q,z}(z) = \dot{E} / S_{xy}(z)$, which leads to the local Fourier law

$$\dot{E} / S_{xy}(z) = -\lambda \nabla_z T(z). \tag{2}$$

The integration of Eq. (2) with respect to z gives the following temperature profile

$$T(z) = T(z_c) - \frac{\dot{E}}{\lambda\pi}\frac{2}{d}\operatorname{arctanh}\left[\frac{2(z - z_c)}{d}\right]. \tag{3}$$

Thermal conductivity λ was determined by fitting Eq. (3) to the temperature profile in the gap region obtained from the NEMD simulation, where $T(z_c)$ and λ were the fitting parameters.

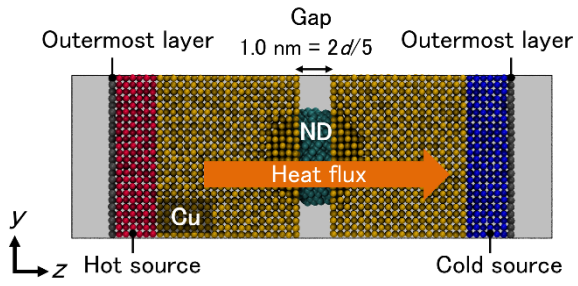

Fig. 1. Our ND–Cu composite system for NEMD simulation.

3. Results and discussion

3.1 Thermal conductivity of bulk diamond crystal

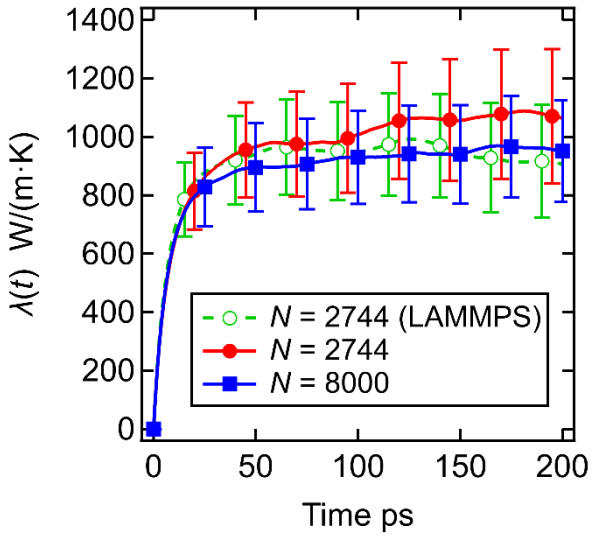

Fig. 2. Thermal conductivity of bulk diamond crystal calculated by AIREBO potential for the systems with 2744 and 8000 atoms. The curve computed with the original heat flux formula of LAMMPS is also included for comparison.

In Fig. 2, the running thermal conductivity described in Eq. (1) for bulk diamond crystal is plotted as a function of time. The thermal conductivity for the systems of 2744 and 8000 atoms were calculated to be 1.08 ± 0.22 kW/(m·K) and 0.96 ± 0.17 kW/(m·K), respectively, and the result was not significantly dependent on the system size as is usually the case for the EMD method [26]. These values of thermal conductivity calculated with AIREBO potential are rather small in comparison with ~3 kW/(m·K) observed for an isotopically pure diamond crystal [34]. It was reported that EMD computations with Tersoff and Brenner potentials also result in a low thermal conductivity as ~2 kW/(m·K) [26] and ~1.2 kW/(m·K) [35], respectively. Thus, this underestimation can be considered a common feature of reactive potentials and should be taken into account when the thermal conductivity derived from these potentials are compared with the experimental ones. Turney et al. [36] clearly demonstrated that thermal conductivity of a crystalline material is significantly underestimated when one assumes the classical

Boltzmann distribution, instead of the Bose-Einstein distribution, for the energy distribution of phonons. The lack of quantum effect in phonon energy distribution is a possible reason for the underestimation.

The above results of AIREBO potentials were obtained using the modified heat flux formula. For comparison, we performed the same computation using the original formula of LAMMPS. The result is also included in Fig. 2. The thermal conductivity was calculated to be 0.92 ± 0.19 kW/(m·K) and eventually, in the case of EMD method, the result was not sensitive to which formula is used. However, the NEMD simulation of diamond shows that the LAMMPS original formula does not satisfy energy conservation as described in Appendix B.

3.2 Structure of nanodiamonds

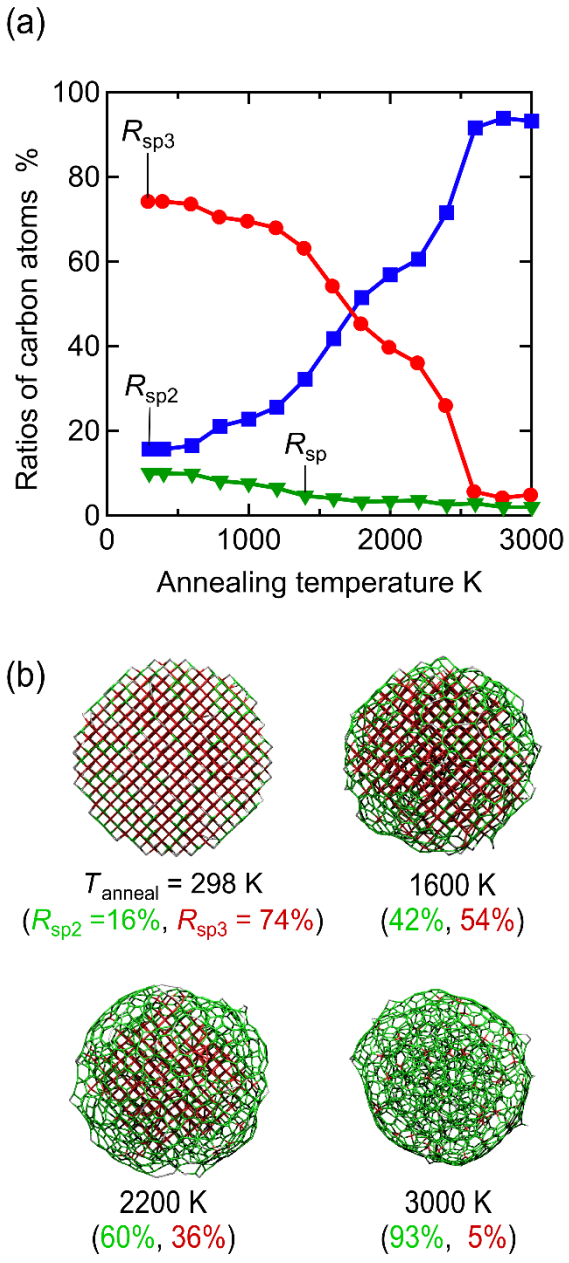

Fig. 3. (a) Ratio of sp-like, sp^2-like, and sp^3-like (2-, 3-, and 4-coordinate) carbons, R_{sp}, R_{sp2}, and R_{sp3}, respectively, to the total number of carbon atoms as a function of annealing temperature. (b) Snapshots of a 2.5 nm nanodiamond obtained by annealing at various temperature.

The 2.5 nm ND changed its structure depending on the annealing temperature T_{anneal}. Figure 3(a)

plots the fractions of carbon atoms with different bond orders as a function of T_{anneal}. Here, the bond order was distinguished by the coordination number within a predetermined coordination radius. The coordination radius was chosen to be 2.0 Å based on radial distribution function [37] so as to reasonably distinguish the bonding and non-bonding states. In the present study, for convenience, a carbon atom is called sp-like, sp^2-like, and sp^3-like carbon, when its coordination number is 2, 3, and 4, respectively. These bonding states are only approximate representations of actual sp, sp^2, and sp^3 bonds. For example, the bonding state of a 3-coordinate carbon on the ND surface may be sp^3 bond with one dangling bond, rather than sp^2 bond, but the above definition does not distinguish these states. Therefore, we put the suffix -like. As shown in Fig. 3(a), the ND was composed mostly of sp^2-like and sp^3-like carbons and only small amount of sp-like carbons, indicating that the structural change is mainly caused by an sp^3-like carbon changing to an sp^2-like carbon.

Examples of the ND structure were shown in Fig. 3 (b). At T_{anneal} = 298 K, most atoms formed sp^3-like bonds and a diamond lattice was maintained well except a weak surface reconfiguration. As T_{anneal} increases, the breaking of sp^3-like bonds, which initiated from the surface, gradually permeated the interior. In the intermediate T_{anneal} from 1600 to 2200 K, the ND had a core–shell structure where core sp^3-like carbons are covered with surface sp^2-like carbons. For higher T_{anneal}, the ND was an amorphous structure composed of randomly oriented sp^2-like bonds. The onion structure was not clear in our NDs obtained by AIREBO potentials whereas it was observed in previous MD studies using REBO [4,10,11] and ReaxFF [12] potentials. According to Brodka et al. [10], a crucial factor for generating the onion structure is to break the sp^3 bonds between neighboring {111} planes of diamond lattice. It is conjectured that the vdW attraction, which is missing in REBO and ReaxFF, disturbed this bond breaking.

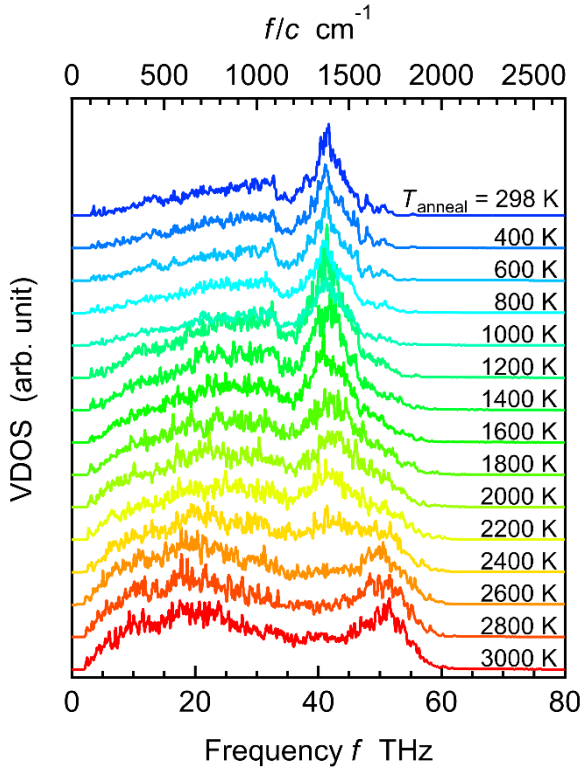

Fig. 4. Vibration density of states (VDOS) of 2.5 nm nanodiamonds at 298 K obtained by annealing at various temperature T_{anneal}. The spectra are vertically shifted for clarity. In the top axis, frequency is converted to the wavenumber of light and c is the speed of light for comparison to the experimental results.

The structural feature shown in Fig. 3 was clearly reflected on the vibration density of states (VDOS), which was calculated as the Fourier transform of the velocity autocorrelation function. The characteristic vibration modes in diamond films or diamond particles of nano- to submicrometer scales have been studied by Raman spectroscopy [9,38–40]. These studies show that the Raman peaks associated with sp^3 carbons are found at around 1320 (diamond peak) – 1380 cm^{-1} (D-band) whereas those associated with sp^2 carbons are at around 1480–1660 cm^{-1} (G-band). The VDOS in our case is shown in Fig. 4. The peak at ~1400 cm^{-1} for T_{anneal} = 298 K is considered the sp^3 peak and as T_{anneal} increases, this peak is gradually attenuated and replaced by the sp^2 peak at around 1700 cm^{-1}. Although the locations of the sp^2 and sp^3 peaks obtained here with AIREBO potential seem slightly higher than those observed in the experiments, the discrepancy is small and the result is considered to be reasonable. The result in Fig. 4

shows that NDs with systematically different structures were obtained with different annealing temperature.

3.3 Thermal conductivity of nanodiamonds

A temperature profile in the ND–Cu composite system for the case of T_{anneal} = 298 K is shown in Fig. 5 as an example. The local temperature was calculated along the z direction for the slabs of width Δz = 2.0 Å. As shown in Fig. 5 (a), the system showed a temperature jump at the ND–copper interface. The corresponding interfacial thermal resistance R was roughly estimated as $R \sim \Delta T S_{xy} / \dot{E} = 6.8 \times 10^{-9}$ m^{2}K/W. Here, the contact area was approximated by the x–y cross section at the edge of the gap region, $S_{xy}(z_{\mathrm{c}} \pm d/5) = 21\pi d^2/100$. The temperature jump at the center of ND in the z direction was defined as $2\Delta T$, which was estimated by extrapolating the temperature profiles of the left and right copper blocks to z_{c}. Although this estimation is crude, the order of R is similar to those of typical metal–diamond interfaces, which were observed to be in the range of 10^{-9}–10^{-8} m^{2}K/W [41]. We do not discuss the thermal conductivity of the copper block since the electronic heat conduction, which explains a large part of heat conduction in copper, is not considered by classical MD simulation. We note that the above result of interfacial thermal resistance is satisfactory at the current stage since our focus is on the thermal conductivity of an ND and the copper block was introduced as a tool to avoid the direct heating of ND.

The magnified view of the temperature profile in the ND region is shown in Fig. 5(b) together with the result of fitting using Eq. (3). The fitting gave the thermal conductivity, $\lambda = 28 \pm 3$ W/(m·K), for the case with T_{anneal} = 298 K. Although the fitted curve was based on the temperature profile in the gap region only, its extrapolation reasonably represents the results for the non-gap regions where the ND is embedded in the Cu block. However, we found that the fitting becomes unstable if the data in the regions far from the gap were included because Eq. (3) diverges as approaching to the z-edges of ND ($z = z_{\mathrm{c}} \pm d/2$). Thus, Eq. (3) is likely to work well for the whole ND, but in the fitting, it is safe to include only the

data in the gap region. The success of Eq. (3) demonstrates that the law of heat conduction in such a nanoscale sphere has a significant similarity to that for a macroscopic sphere, and we consider that it is possible to apply the concept of thermal conductivity to the ND.

In order to examine the effect of copper block size in the heat flow direction, we carried out the same NEMD simulation for T_{anneal} = 298 K using copper blocks twice in length in the z direction. The thermal conductivity for this elongated system was calculated as 35 ± 6 W/(m·K), which seems slightly higher than 28 ± 3 W/(m·K) for the original size. However, the difference is not significant compared with the statistical uncertainty in the present study. Therefore, we consider that the original size of copper crystal is adequate.

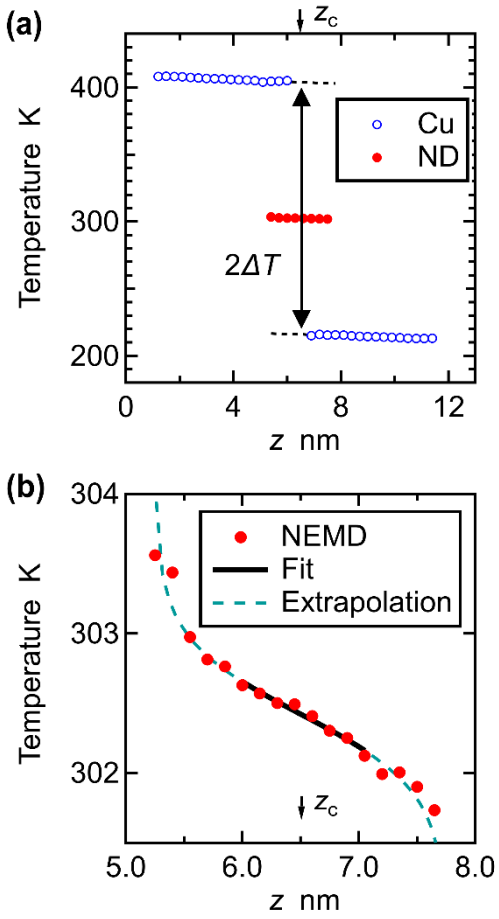

Fig. 5. (a) Temperature profile along the direction of the heat conduction (the z direction) formed in the ND–Cu composite system for T_{anneal} = 298 K. The dashed line is the

extrapolation of the copper temperature profile. (b) Magnified view of the ND region. The result of fit with Eq. (3) over the gap region ($6.0 \leq z \leq 7.0$ nm) and its extrapolation to the outer regions are also shown.

The thermal conductivity of the 2.5 nm ND thus calculated is shown in Fig. 6 as a function of the ratio of sp^2-like carbons, R_{sp2}. The value varies approximately from 10 to 28 W/(m·K) depending on R_{sp2}. These values are two orders of magnitude lower than that of bulk diamond computed in Section 3.1, representing the size effect due to the ballistic heat transfer [15]. The diamond-like NDs tend to exhibit higher thermal conductivity than amorphous ones. The experimental values reported for the thermal conductivity of NDs are lower than these values. Kidalov et al. used a steady-state method and measured the thermal conductivity of a sintered powder of NDs with average diameter of 5 nm to be $\lambda \sim 8.5$ W/(m·K) [42]. The Laser flash measurements of Vlasov et al. showed $\lambda = 0.3$–1.7 W/(m·K) for the composites where NDs with average diameter of 6 nm were dispersed in the matrix of sp^2 carbon [43]. These lower values from experiments are not inconsistent with our results because they include the thermal resistance due to voids and grain boundaries. The present results therefore offer the upper limit for the thermal conductivity of a 2.5 nm ND, but a real ND possibly has a higher value if the discussion regarding the underestimation by AIREBO potential in Section 3.1 is also valid for the 2.5 nm NDs.

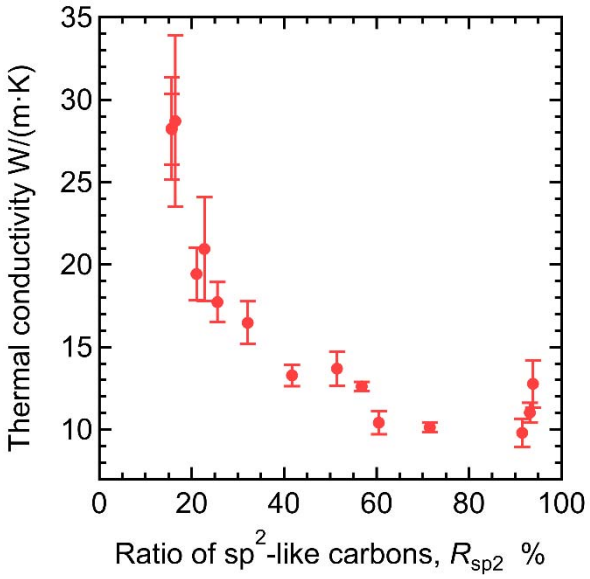

Fig. 6. Thermal conductivity of a 2.5 nm nanodiamond as a function of the ratios of sp^2-like (3-coordinate) carbons.

3.4 Relevance to the internal structures of ND

We examined the relationship between the structural dependence of thermal conductivity in Fig. 6 and the properties of C–C bond, which is the main path of heat transfer in ND. The numbers of C–C bonds in sp^2-like and sp^3-like configurations were calculated as $3n_{sp2}/2$ and $4n_{sp3}/2$ from the number of sp^2-like and sp^3-like carbons in a single ND, n_{sp2} and n_{sp3}, respectively. The results are shown in Fig. 7(a) both as a function of R_{sp2}. It is found that the number of sp^2-like bonds exceeds that of sp^3-like ones at R_{sp2} ~ 60%. In other words, the major path for heat transfer switches at this threshold ratio from sp^3-like bond to sp^2-like bond. Correspondingly, in Fig. 6, the decrease in thermal conductivity with R_{sp2} is suppressed after this threshold ratio. It is thus likely that the trends before and after the threshold seen in Fig. 6 reflect the nature of the major heat path in each region of R_{sp2}.

The heat transfer capability of a single C–C bond in sp^3-like and sp^2-like configurations were approximately estimated on the basis of the atomistic heat path analysis [44]. In the present case, thermal

conductivity can be reasonably expressed as $\lambda = \sum_{X=\mathrm{sp,sp2,sp3}} \rho_X \Lambda_X$, where ρ_X is the number density of C–C bonds in the space and Λ_X is the efficiency of heat transfer per single C–C bond, i.e., the contribution of thermal energy transfer via each interatomic bond to thermal conductivity. The efficiency of a sp^3-like C–C bond, Λ_{sp3}, was estimated from the result for T_{anneal} = 298 K, where the ratio of sp^3-like carbons was 74%. In this case, the thermal conductivity was approximated as $\lambda \sim \rho_{sp3}\Lambda_{sp3}$, where $\lambda = 28 \pm 3$ W/(m·K) and $\rho_{sp3} = 0.524$ Å^{-3}, and the path efficiency was evaluated to be $\Lambda_{sp3} = 5.3 \times 10^{-29}$ Wm^2/K. Similarly, for sp^2-like bond, the thermal conductivity of the ND for T_{anneal} = 3000 K with the ratio of sp^2-like carbons of 93% was approximated as $\lambda \sim \rho_{sp2}\Lambda_{sp2}$. We obtained $\Lambda_{sp2} = 2.23 \times 10^{-29}$ Wm^2/K with $\lambda = 11.0 \pm 0.6$ W/(m·K) and $\rho_{sp2} = 0.494$ Å^{-3}. This rough estimation implies that the heat transfer through an sp^3-like bond is more efficient than that via an sp^2-like bond. This result suggests a possible mechanism by which thermal conductivity increases with increasing size of nanoparticle, because sp^2-like carbons are rich in the surface shell, and the surface-to-volume ratio decreases with the nanoparticle size. However, the effect of ballistic phonon, which increases thermal conductivity of nanocrystal almost linearly with crystal size [45], would be the major reason for the size dependence. We note that the efficiency of the order of 10^{-29} Wm^2/K is two orders of magnitude higher than those of C–C bonds in the hydrocarbon chains of alkanes and alcohols in their liquid states [44,46].

We also examined the orientations of C–C bonds in terms of angle θ between the bond axis and the heat conduction direction (z-axis) as shown in Fig. 7(b), where the angle in the range $0 \le \cos\theta \le 1$ was considered using the fact that $\cos\theta$ and $-\cos\theta$ indicate equivalent orientations. It is expected that a single C–C bond most effectively contributes the total heat conduction when $\cos\theta = 1$ and the contribution decreases with decreasing $\cos\theta$. It can be seen from Fig. 7(b) that as R_{sp2} increases, the distribution of $\cos\theta$ gradually loses its peaks found at the orientation of sp^3-like bonds and becomes more uniform. This orientational disorder can enhance the phonon scattering. In addition, the average value of $\cos\theta$ decreases. This result indicates that in the amorphous sp^2-like state, the orientation of C–C bond deviates slightly more from the heat conduction axis than in the diamond-like state. The phonon scattering enhanced by

the orientational disorder and the mismatch between the bond direction and the heat conduction may provide a possible reason for the lower path efficiency of sp^2-like bond compared with that of sp^3-like one.

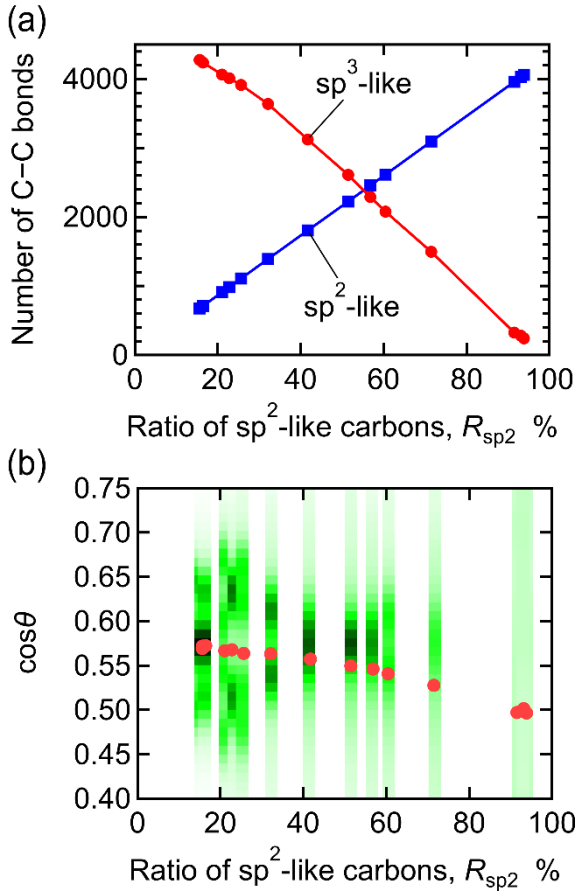

Fig. 7. (a) Number of C–C bonds in a 2.5 nm nanodiamond and (b) average orientation (red circles) of C–C bond, both as a function of the ratio of sp^2-like (3-coordinate) carbons. In subfigure (b), θ is the angle between C–C bond and the heat conduction direction (the z-axis of the system). The green color shows the distribution of $\cos\theta$ and the darker the color is, the higher the distribution.

Based on the discussion above, we interpret the result in Fig. 6 as follows. For $R_{sp2} \leq 60\%$, the core of sp^3-like diamond structure constitutes the major part of ND. The decreasing trend of the thermal conductivity in this region is explained by the shortening of phonon mean-free-path associated with the

shrink of the diamond lattice core. For larger R_{sp2}, the domain of amorphous sp^2-like carbons predominates that of sp^3-like carbons. In this case, the phonon mean-free-path is sufficiently short because the random orientation of C–C bonds enhances phonon scattering and a further increase of sp^2-like bonds does not significantly change the length of mean-free-path. Thus, the dependence of thermal conductivity on R_{sp2} becomes weak as is shown in Fig. 6.

In terms of atomistic heat path, the trend in Fig. 6 can be qualitatively explained by the fact that efficient heat paths (sp^3-like bonds) are replaced with less efficient ones (sp^2-like bonds) with increasing R_{sp2}. However, a linear combination of the contributions from sp^2-like and sp^3-like bonds as $\lambda = \rho_{sp2}\Lambda_{sp2} + \rho_{sp3}\Lambda_{sp3}$ seems too simple to describe quantitatively the overall trend in Fig. 6 and further study is necessary to refine the estimation formula based on the atomistic heat path.

4. CONCLUSIONS

We investigated the structural dependence of thermal conductivity of a spherical ND with 2.5 nm in diameter. To this aim, we proposed here the NEMD simulation of a composite system, instead of conventional methods that fail to evaluate the thermal conductivity of nanoscale materials. The ND had a core-shell structure where a diamond core is surrounded by the shell of sp^2-like (3-coordinate) carbons and the thermal conductivity varied from 10 to 28 W/(m·K) depending on the ratios of sp^3-like or sp^2-like carbons. From the consideration of heat transfer due to a single C–C bond, we suggested that the thermal conductivity of ND reflects the heat transfer characteristics of an sp^3-like or sp^2-like bond, whichever is richer. In the present case, a C–C bond performed heat transfer more effectively when it was in sp^3-like configuration than in sp^2-like one, and therefore an ND with a larger diamond core tends to display a higher thermal conductivity. There are some issues that remain to be solved, such as the effects of force fields and the validity of approximations in calculating the thermal conductivity. Nevertheless, the present study provides useful insights into the heat conduction in nanocarbon materials and how to analyze it.

The thermal conductivity obtained here is also useful as reference values for comparison with those derived from other computational methods and experiments.

ACKNOWLEDGMENTS

This work was partly supported by JST-CREST Grant Number JPMJCR17I2, Japan. Computational simulations were performed on the supercomputer system “AFI-NITY” at the Advanced Fluid Information Research Center, Institute of Fluid Science, Tohoku University.

APPENDIX A

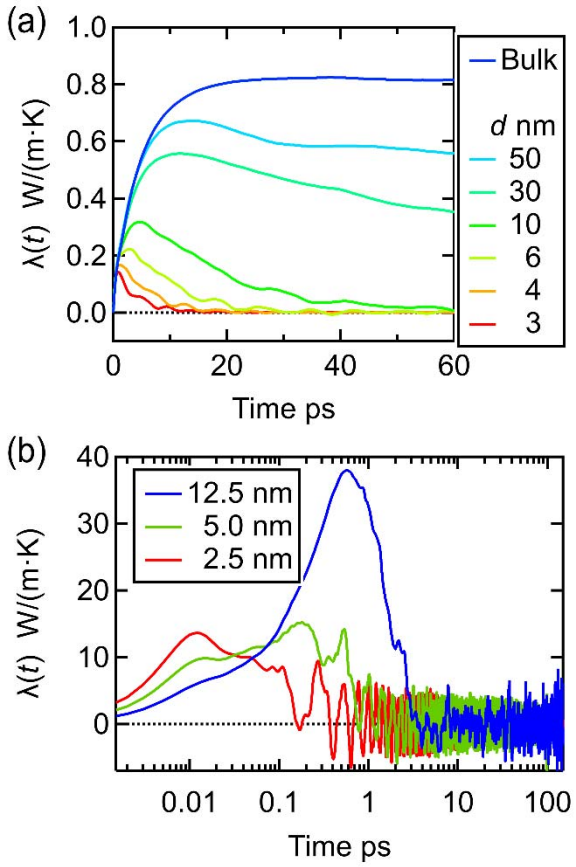

Fig. A1. Running thermal conductivity as a function of time. (a) For a spherical cluster of argon fcc crystal at 30 K for various diameters d = 3–50 nm. The curve for the bulk fcc crystal is also included. (b) For a spherical nanodiamond with d = 2.5–12.5 nm at 298 K.

As described in the text, the MD calculation of thermal conductivity based on the Green-Kubo formula cannot be applied to a free nanoparticle system. In this appendix, we shortly illustrate this. For clarity, we first consider a system with a well-established pair potential, i.e., the system of a spherical nanoparticle of fcc argon crystal under the free boundary conditions in all directions. The LJ potential was used for Ar–Ar interaction with σ_{ArAr} = 3.41Å, ε_{ArAr} = 0.238 kcal/mol [47], and cutoff length of 12 Å. After an equilibration run at 30 K, the running thermal conductivity $\lambda(t)$ as described in Eq. (1) was calculated by performing a 20 ns constant *NVE* run with the timestep of 2 fs. The nanoparticles of several

sizes with diameters 3–50 nm were examined. For comparison, $\lambda(t)$ for the bulk fcc crystal, composed of 10 × 10 × 10 unit cells under the three-dimensional periodic boundary conditions, was also computed. The results are illustrated in Fig. A1(a). In the case of a nanoparticle, heat flow changes its sign by the reflection at the edge of the nanoparticle, and these forward and backward flows cancel with each other. As a result, the $\lambda(t)$ of a nanoparticle falls down to zero after the time required for a thermal energy to make a round trip across the nanoparticle. The larger the nanoparitcle size, the longer the round-trip time, and the curve approaches more to that of the bulk crystal. The same computation for the 2.5 nm ND for T_{anneal} = 298 K is shown in Fig. A1(b). We also included the results for the larger NDs with d = 5 nm and 12.5 nm equilibrated at 298 K without annealing. The results are essentially the same as those of argon if heat flux is calculated with the modified formula explained in Appendix B, although the curves of $\lambda(t)$ are much more complicated because of strong vibrations of C–C bonds. These results demonstrate that the conventional Green–Kubo formalism cannot be applied to a nanoparticle.

APPENDIX B

In the present study, we modified the LAMMPS code of heat flux calculation so as to follow the law of energy conservation and this appendix describes the modified expression of heat flux and its validation. In AIREBO potential, the total internal energy E_{tot} of an N particle system is given by

$$E_{\text{tot}} = \sum_{i=1}^{N} K_i + \frac{1}{2}\sum_{i=1}^{N}\sum_{j\neq i}^{N} U_{ij}\,, \tag{B1}$$

where $K_i = m_i \mathbf{v}_i^2 / 2$, m_i, and $\mathbf{v}_i = (v_{x,i}, v_{y,i}, v_{z,i})$ are the per-atom kinetic energy, mass, and velocity vector of atom i, respectively. The pair potential between atoms i and j, U_{ij}, is actually a function of all atoms k and l that are the neighbors of i and j, respectively, and is in general asymmetric as $U_{ij} \neq U_{ji}$. The choice of per-atom potential energy U_i is somewhat arbitrary because there is no strict criterion for dividing U_{ij} into the contributions of atoms i and j. For any form of U_i, it is possible to derive the corresponding heat flux expression that satisfies energy conservation and it has been reported that the results are not

significantly dependent on the choice of U_i [15,26]. Here, we use a symmetrical form for the per-atom potential energy U_i:

$$U_i = \frac{1}{4}\sum_{j\neq i}^{N}(U_{ij} + U_{ji}), \tag{B2}$$

following the definition adopted in LAMMPS.

Suppose a flat control surface at $z = z_s$ whose normal is in the z direction and thereby the system is separated into the left and right sub-volumes. In order to satisfy energy conservation, the amount of energy $J_z(z_s)S_{xy}$ passed through the control surface must be equal to the energy increase rate in the right volume [48], which in the present case leads to

$$J_z(z_s)S_{xy} = \frac{d}{dt}\left[\sum_{i=1} E_i\theta(z_{is})\right] = \sum_{i=1} E_i v_{z,i}\delta(z_{is}) - \sum_i\sum_{j\neq i}\frac{\partial U_j}{\partial \mathbf{r}_i}\cdot\mathbf{v}_i\left[\theta(z_{is}) - \theta(z_{js})\right], \tag{B3}$$

where $J_z(z_s)$ is the heat flux in the z direction measured at the control surface; S_{xy} is the x–y cross section of the control surface; $E_i = K_i + U_i$; $\mathbf{r}_i = (x_i, y_i, z_i)$ is the position vector of atom i; $z_{is} = z_i - z_s$; θ is the Heaviside step function; and δ is the delta function. The average heat flux J_z in a control volume $V = S_{xy}\Delta z$ is obtained by integrating Eq. (B3) with respect to z_s over Δz as,

$$J_z V = \sum_{i\in V} E_i v_{z,i} - \sum_i\sum_{j\neq i}\frac{\partial U_j}{\partial \mathbf{r}_i}\cdot\mathbf{v}_i z_{ij}^*, \tag{B4}$$

where z_{ij}^* means the portion of $z_i - z_j$ that is contained in the control volume. After some manipulations, the second term in the right-hand side of Eq. (B4) can be expressed in a highly compatible form with LAMMPS code as follows

$$\begin{aligned}-\sum_{i=1}^{N}\sum_{j\neq 1}^{N}\frac{\partial U_j}{\partial \mathbf{r}_i}\mathbf{v}_i z_{ij}^* = \frac{1}{2}\sum_i\sum_{j\neq i}\frac{1}{2}\Big[\; & z_{ij}^*\mathbf{f}_{i,ij}\cdot\mathbf{v}_i - z_{ij}^*\mathbf{f}_{j,ij}\cdot\mathbf{v}_j \\ & + \sum_{k\neq i,j}\left\{z_{ij}^*\mathbf{f}_{i,ijk}\cdot\mathbf{v}_i - z_{ij}^*\mathbf{f}_{j,ijk}\cdot\mathbf{v}_j - (z_{ik}^* + z_{jk}^*)\mathbf{f}_{k,ijk}\cdot\mathbf{v}_k\right\} \\ & + \sum_{k\neq i,j}\sum_{l\neq i,j}\left\{z_{ij}^*\mathbf{f}_{i,ijkl}\cdot\mathbf{v}_i - z_{ij}^*\mathbf{f}_{j,ijkl}\cdot\mathbf{v}_j - (z_{ik}^* + z_{jk}^*)\mathbf{f}_{k,ijkl}\cdot\mathbf{v}_k - (z_{il}^* + z_{jl}^*)\mathbf{f}_{l,ijkl}\cdot\mathbf{v}_l\right\}\;\Big],\end{aligned} \tag{B5}$$

where $\mathbf{f}_{i,ij}$ is the two-body force on atom i, which is dependent on atoms i and j, and similarly $\mathbf{f}_{i,ijk}$ and $\mathbf{f}_{i,ijkl}$ are the three- and four-body forces, respectively, and these forces are already available in LAMMPS.

In order to validate the modified heat flux formula, we performed the NEMD simulation of bulk

diamond crystal with 6 × 6 × 40 unit cells at 298 K under the constant heat flux of 10 GW/m^2 using EHEX [33]. After an equilibration of several ns, the cumulative average of heat flux, $\langle J_z(t) \rangle = \int_0^t J_z(s)ds / t$, was computed and the result is plotted in Fig. B1. For comparison, the same computation was performed using the original LAMMPS formula. As shown in Fig. B1, the average heat flux calculated with the modified formula correctly converged to the imposed value of 10 GW/m^2, whereas the curve with the LAMMPS formula still fluctuates around the imposed value within the time scale examined. Discrepancy between the measured flux and the imposed one when using the LAMMPS formula and many-body potentials has also been reported for two dimensional crystalline materials [49,50]. The results confirm that the modified formula satisfies energy conservation.

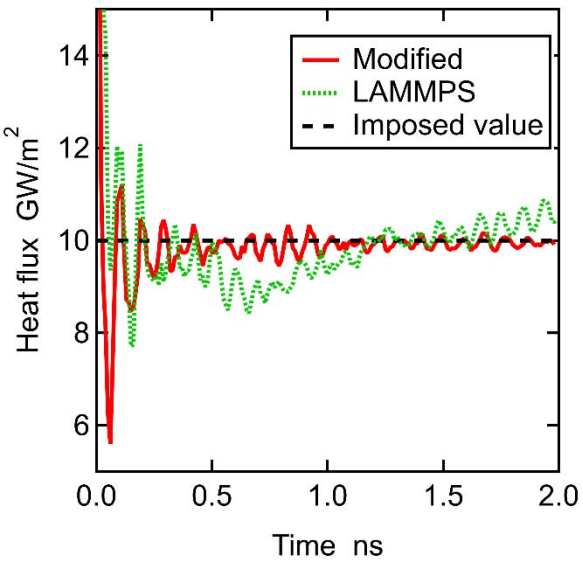

Fig. B1. Cumulative average of heat flux as a function of time calculated with our modified expression of heat flux and that with the original LAMMPS formula. The dashed line shows the value of heat flux imposed on the system.

REFERENCES

[1] F. Mashali, E.M. Languri, J. Davidson, D. Kerns, W. Johnson, K. Nawaz, G. Cunningham, Thermo-physical properties of diamond nanofluids: A review, Int. J. Heat Mass Transf. 129 (2019) 1123–1135. doi:10.1016/j.ijheatmasstransfer.2018.10.033.

[2] V.N. Mochalin, Y. Gogotsi, Nanodiamond-polymer composites, Diam. Relat. Mater. 58 (2015) 161–171. doi:10.1016/j.diamond.2015.07.003.

[3] K. Pietrak, T.S. Winiewski, A review of models for effective thermal conductivity of composite materials, J. J. Power Technol. 95 (2015) 14–24. doi:10.1109/TPAMI.1986.4767851.

[4] A. Bródka, Ł. Hawełek, A. Burian, S. Tomita, V. Honkimäki, Molecular dynamics study of structure and graphitization process of nanodiamonds, J. Mol. Struct. 887 (2008) 34–40. doi:10.1016/j.molstruc.2008.01.055.

[5] Y. Zhang, K.Y. Rhee, D. Hui, S.J. Park, A critical review of nanodiamond based nanocomposites: Synthesis, properties and applications, Compos. Part B Eng. 143 (2018) 19–27. doi:10.1016/j.compositesb.2018.01.028.

[6] Y. V. Butenko, V.L. Kuznetsov, A.L. Chuvilin, V.N. Kolomiichuk, S. V. Stankus, R.A. Khairulin, B. Segall, Kinetics of the graphitization of dispersed diamonds at “low” temperatures, J. Appl. Phys. 88 (2000) 4380. doi:10.1063/1.1289791.

[7] S. Tomita, M. Fujii, S. Hayashi, Optical extinction properties of carbon onions prepared from diamond nanoparticles, Phys. Rev. B. 66 (2002) 245424. doi:10.1103/PhysRevB.66.245424.

[8] K. Bogdanov, A. Fedorov, V. Osipov, T. Enoki, K. Takai, T. Hayashi, V. Ermakov, S. Moshkalev, A. Baranov, Annealing-induced structural changes of carbon onions: High-resolution transmission electron microscopy and Raman studies, Carbon N. Y. 73 (2014) 78–86. doi:10.1016/j.carbon.2014.02.041.

[9] J. Xiao, G. Ouyang, P. Liu, C.X. Wang, G.W. Yang, Reversible nanodiamond-carbon onion phase transformations, Nano Lett. 14 (2014) 3645–3652. doi:10.1021/nl5014234.

[10] A. Bródka, T.W. Zerda, A. Burian, Graphitization of small diamond cluster -- Molecular dynamics simulation, Diam. Relat. Mater. 15 (2006) 1818–1821. doi:http://dx.doi.org/10.1016/j.diamond.2006.06.002.

[11] L. Hawelek, A. Brodka, S. Tomita, J.C. Dore, V. Honkimäki, A. Burian, Transformation of nano-diamonds to carbon nano-onions studied by X-ray diffraction and molecular dynamics, Diam. Relat. Mater. 20 (2011) 1333–1339. doi:10.1016/j.diamond.2011.09.008.

[12] P. Ganesh, P.R.C. Kent, V. Mochalin, Formation, characterization, and dynamics of onion-like carbon structures for electrical energy storage from nanodiamonds using reactive force fields, J. Appl. Phys. 110 (2011) 73506. doi:10.1063/1.3641984.

[13] G. Ostroumova, N. Orekhov, V. Stegailov, Reactive molecular-dynamics study of onion-like carbon nanoparticle formation, Diam. Relat. Mater. 94 (2019) 14–20. doi:10.1016/j.diamond.2019.01.019.

[14] V.B. Efimov, L.P. Mezhov-Deglin, Phonon scattering in diamond films, Phys. B Condens. Matter. 263–264 (1999) 745–748. doi:10.1016/S0921-4526(98)01280-0.

[15] P.K. Schelling, S.R. Phillpot, P. Keblinski, Comparison of atomic-level simulation methods for computing thermal conductivity, Phys. Rev. B. 65 (2002) 144306. doi:10.1103/PhysRevB.65.144306.

[16] E.A. Algaer, F. Müller-Plathe, Molecular dynamics calculations of the thermal conductivity of molecular liquids, polymers, and carbon nanotubes, Soft Mater. 10 (2012) 42–80. doi:10.1080/1539445X.2011.599699.

[17] S.S. Mahajan, G. Subbarayan, B.G. Sammakia, Estimating thermal conductivity of amorphous silica nanoparticles and nanowires using molecular dynamics simulations, Phys. Rev. E. 76 (2007) 056701. doi:10.1103/PhysRevE.76.056701.

[18] K. Termentzidis, V.M. Giordano, M. Katsikini, E. Paloura, G. Pernot, M. Verdier, D. Lacroix, I. Karakostas, J. Kioseoglou, Enhanced thermal conductivity in percolating nanocomposites: A

molecular dynamics investigation, Nanoscale. 10 (2018) 21732–21741. doi:10.1039/c8nr05734f.

[19] Q. Zou, M.Z. Wang, Y.G. Li, Analysis of the nanodiamond particle fabricated by detonation, J. Exp. Nanosci. 5 (2010) 319–328. doi:10.1080/17458080903531021.

[20] A.N. Panova, V.Y. Dolmatov, E. V. Ishchenko, G.G. Tsapyuk, A.A. Bochechka, M. V. Veretennikova, V. Myllymaki, E. V. Nikitin, The influence of synthesis conditions on the surface state of detonation nanodiamonds, J. Superhard Mater. 37 (2015) 202–210. doi:10.3103/S1063457615030089.

[21] S. Plimpton, Fast Parallel Algorithms for Short-Range Molecular Dynamics, J. Comput. Phys. 117 (1995) 1–19. doi:10.1006/jcph.1995.1039.

[22] S.J. Stuart, A.B. Tutein, J.A. Harrison, A reactive potential for hydrocarbons with intermolecular interactions, J. Chem. Phys. 112 (2000) 6472–6486. doi:10.1063/1.481208.

[23] J. Tersoff, Empirical Interatomic Potential for Carbon, with Applications to Amorphous Carbon, Phys. Rev. Lett. 61 (1988) 2879–2882. doi:10.1103/PhysRevLett.61.2879.

[24] D.W. Brenner, Empirical potential for hydrocarbons for use in simulating the chemical vapor deposition of diamond films, Phys. Rev. B. 42 (1990) 9458–9471. doi:10.1103/PhysRevB.42.9458.

[25] M.E. Tuckerman, J. Alejandre, R. López-Rendón, A.L. Jochim, G.J. Martyna, A Liouville-operator derived measure-preserving integrator for molecular dynamics simulations in the isothermal-isobaric ensemble, J. Phys. A. Math. Gen. 39 (2006) 5629–5651. doi:10.1088/0305-4470/39/19/S18.

[26] Z. Fan, L.F.C. Pereira, H.-Q. Wang, J.-C. Zheng, D. Donadio, A. Harju, Force and heat current formulas for many-body potentials in molecular dynamics simulations with applications to thermal conductivity calculations, Phys. Rev. B. 92 (2015) 94301. doi:10.1103/PhysRevB.92.094301.

[27] D. Surblys, H. Matsubara, G. Kikugawa, T. Ohara, Application of atomic stress to compute heat

flux via molecular dynamics for systems with many-body interactions, Phys. Rev. E. 99 (2019) 51301. doi:10.1103/PhysRevE.99.051301.

[28] P. Boone, H. Babaei, C.E. Wilmer, Heat Flux for Many-Body Interactions: Corrections to LAMMPS, J. Chem. Theory Comput. 15 (2019) 5579–5587. doi:10.1021/acs.jctc.9b00252.

[29] M.I. Baskes, Modified embedded-atom potentials for cubic materials and impurities, Phys. Rev. B. 46 (1992) 2727–2742. doi:10.1103/PhysRevB.46.2727.

[30] A.K. Rappe, C.J. Casewit, K.S. Colwell, W.A. Goddard, W.M. Skiff, UFF, a full periodic table force field for molecular mechanics and molecular dynamics simulations, J. Am. Chem. Soc. 114 (1992) 10024–10035. doi:10.1021/ja00051a040.

[31] D. Wolf, J.F. Lutsko, Structurally-induced elastic anomalies in a superlattice of (001) twist grain boundaries, J. Mater. Res. 4 (1989) 1427–1443. doi:10.1557/JMR.1989.1427.

[32] Y. Guo, W. Guo, Structural transformation of partially confined copper nanowires inside defected carbon nanotubes, Nanotechnology. 17 (2006) 4726–4730. http://stacks.iop.org/0957-4484/17/i=18/a=033.

[33] P. Wirnsberger, D. Frenkel, C. Dellago, An enhanced version of the heat exchange algorithm with excellent energy conservation properties, J. Chem. Phys. 143 (2015) 124104. doi:http://dx.doi.org/10.1063/1.4931597.

[34] L. Wei, P.K. Kuo, R.L. Thomas, T.R. Anthony, W.F. Banholzer, Thermal conductivity of isotopically modified single crystal diamond, Phys. Rev. Lett. 70 (1993) 3764–3767. doi:10.1103/PhysRevLett.70.3764.

[35] J. Che, T. Çağın, W. Deng, W.A.G. III, Thermal conductivity of diamond and related materials from molecular dynamics simulations, J. Chem. Phys. 113 (2000) 6888–6900. doi:10.1063/1.1310223.

[36] J.E. Turney, A.J.H. McGaughey, C.H. Amon, Assessing the applicability of quantum corrections to classical thermal conductivity predictions, Phys. Rev. B. 79 (2009) 224305.

doi:10.1103/PhysRevB.79.224305.

[37] W. Li, C. Zou, Experimental investigation of stability and thermo-physical properties of functionalized β-CD-TiO2-Ag nanofluids for antifreeze, Powder Technol. 340 (2018) 290–298. doi:https://doi.org/10.1016/j.powtec.2018.09.005.

[38] J. Cebik, J.K. McDonough, F. Peerally, R. Medrano, I. Neitzel, Y. Gogotsi, S. Osswald, Raman spectroscopy study of the nanodiamond-to-carbon onion transformation, Nanotechnology. 24 (2013) 205703. doi:10.1088/0957-4484/24/20/205703.

[39] M. Chaigneau, G. Picardi, H.A. Girard, J.C. Arnault, R. Ossikovski, Laser heating versus phonon confinement effect in the Raman spectra of diamond nanoparticles, J. Nanoparticle Res. 14 (2012). doi:10.1007/s11051-012-0955-9.

[40] K.W. Sun, J.Y. Wang, T.Y. Ko, Raman spectroscopy of single nanodiamond: Phonon-confinement effects, Appl. Phys. Lett. 92 (2008) 18–21. doi:10.1063/1.2912029.

[41] H.-K. Lyeo, D.G. Cahill, Thermal conductance of interfaces between highly dissimilar materials, Phys. Rev. B. 73 (2006) 144301. doi:10.1103/PhysRevB.73.144301.

[42] S. V. Kidalov, F.M. Shakhov, A.Y. Vul', Thermal conductivity of nanocomposites based on diamonds and nanodiamonds, Diam. Relat. Mater. 16 (2007) 2063–2066. doi:10.1016/j.diamond.2007.07.010.

[43] A. Vlasov, V. Ralchenko, S. Gordeev, D. Zakharov, I. Vlasov, A. Karabutov, P. Belobrov, Thermal properties of diamond/carbon composites, Diam. Relat. Mater. 9 (2000) 1104–1109. doi:10.1016/S0925-9635(99)00256-3.

[44] H. Matsubara, G. Kikugawa, T. Bessho, S. Yamashita, T. Ohara, Effects of molecular structure on microscopic heat transport in chain polymer liquids, J. Chem. Phys. 142 (2015) 164509. doi:http://dx.doi.org/10.1063/1.4919313.

[45] O. Yenigun, M. Barisik, Effect of nano-film thickness on thermal resistance at water/silicon interface, Int. J. Heat Mass Transf. 134 (2019) 634–640.

doi:10.1016/j.ijheatmasstransfer.2019.01.075.

[46] H. Matsubara, G. Kikugawa, T. Bessho, S. Yamashita, T. Ohara, Molecular dynamics study on the role of hydroxyl groups in heat conduction in liquid alcohols, Int. J. Heat Mass Transf. 108 (2017) 749–759. doi:10.1016/j.ijheatmasstransfer.2016.12.045.

[47] M.P. Allen, D.J. Tildesley, Computer simulation of liquids, Oxford University Press, New York, 1987.

[48] D. Torii, T. Nakano, T. Ohara, Contribution of inter- and intramolecular energy transfers to heat conduction in liquids, J. Chem. Phys. 128 (2008) 44504. doi:http://dx.doi.org/10.1063/1.2821963.

[49] M. Gill-Comeau, L.J. Lewis, Heat conductivity in graphene and related materials: A time-domain modal analysis, Phys. Rev. B - Condens. Matter Mater. Phys. 92 (2015) 1–13. doi:10.1103/PhysRevB.92.195404.

[50] K. Xu, Z. Fan, J. Zhang, N. Wei, T. Ala-Nissila, Thermal transport properties of single-layer black phosphorus from extensive molecular dynamics simulations, Model. Simul. Mater. Sci. Eng. 26 (2018). doi:10.1088/1361-651X/aae180.